ACS APPLIED MATERIALS & INTERFACES

Research Article

Cite This: ACS Appl. Mater. Interfaces 2019, 11, 27259−27268

www.acsami.org

Ultrabright Full Color Carbon Dots by Fine-Tuning Crystal Morphology Controllable Synthesis for Multicolor Bioimaging and Sensing

Feng Huo,[†,‡] Yuhang Liu,[†,‡] Mingguang Zhu,[†] En Gao,[§] Bin Zhao,*[,‡,∥] and Xiupei Yang*[,‡]

[†]School of Chemistry and Chemical Engineering, Analytical Testing Center, Institute of Micro/Nano Intelligent Sensing, Neijiang Normal University, Neijiang 641100, PR China

[‡]Chemical Synthesis and Pollution Control Key Laboratory of Sichuan Province, China West Normal University, Nanchong 637000, PR China

[§]State Key Laboratory of Medicinal Chemical Biology, College of Pharmacy and Tianjin Key Laboratory of Molecular Drug Research and [∥]Department of Chemistry, Key Laboratory of Advanced Energy Material Chemistry, MOE, and Collaborative Innovation Center of Chemical Science and Engineering (Tianjin), Nankai University, Tianjin 300350, PR China

Supporting Information

ABSTRACT: In this paper, two kinds of novel carbon nanocrystals (CNCs) with different crystal morphologies (the branch-chain young sprout form (CM1) and conifer-pine form (CM2)) were obtained in a controllable way. The mechanism of crystal morphological development was explored well. When the two kinds of the CNCs were dissolved in different polar solvents, they voluntarily become "ultrafine crystals" at the moment. After that, the ultrabright full color carbon dots (UBFCCDs) have been preliminarily prepared by fine-controlling. With the evaporation of the solvents, the CNCs crystallized again, which could repeat back and forth many times. After the conditions of preparing for CDs were optimized carefully, the as-prepared CDs exhibit ultrabright effects of multiexcitation and multiemission (from blue to red) and can show unique up-conversion luminescence characteristics under a lower excitation wavelength of 660 nm instead of a near-infrared wavelength of 980 or 808 nm. Significantly, the QY% of the UBFCCDs can reach 78.0%, which is higher than that of the traditional hydrothermal methods of discarding precipitation and carrying out dialysis (QY% = 69.0%). The as-prepared CDs can be used for multicolor biomedical imaging in vivo and in vitro and metal ion sensing and also show their potential value for industrial applications.

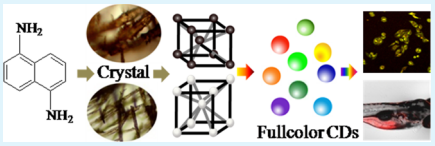

KEYWORDS: *Crystal morphology, Carbon nanocrystals (CNCs), Fine-tuning, Ultrabright full color carbon dots (UBFCCDs), Multicolor bioimaging*

1. INTRODUCTION

In the past few years, there have been an increasing number of studies concerning the syntheses and utilization of fluorescent carbon nanomaterials due to their many unique advantages.[1−6] Carbon nanomaterials such as carbon quantum dots (CDs),[7−10] carbon nanotubes,[11−13] graphene,[14−16] carbon polymerization dots,[17,18] and lanthanide hybrid nanomaterials[19,20] with special structures and unique optical properties have attracted a great deal of attention for applications in chemical sensing,[21−23] biological sensing,[24−26] bioimaging,[27,28] nanomedicine,[29,30] catalysis,[31] and so forth. Specially, the CDs took their fantastic advantages in the fields of bioimaging and biomarkers, including multiple live cell imaging, even tissue imaging of mice and zebrafish in vivo.[32−36] Among the reported synthetic approaches for preparing CDs, recently, the simple and relatively mild experimental conditions or schemes have become a research hotspot more and more, for instance, electrochemical etching,[37−39] ultrasonic-assisted routes,[40−42] microwave,[43−45] refluxing processes,[46] and hydrothermal approaches.[9,47−51] Usually, the hydrothermal method is the better method among them because the one-pot method is facile, fast, and convenient, which has attracted particular attention of researchers in recent years. However, as far as we are aware, most of the conventional hydrothermal approaches generally include some procedures of reaction, discarding sediment and the dialysis. Nearly no attention has been paid to the precious sediment. Furthermore, the FL efficiency of the prepared CDs is much lower after bearing dialysis with a great deal of solvent. Hence, they are very difficult to be used as biomarkers of practical samples due to the fluorescence quenching caused by the complex cell matrix. In addition, if it cannot be preserved for a long time, the industrial application value of CDs shows obvious limitations.

It is worth noting that the controlled crystal morphology and phase of $AgInTe_2$ nanocrystals with UCPL emission characteristics were reported as an expectative fluorescent platform for sensing and imaging.[52,53] Unfortunately, because of the lower QY% and the complex surface modification, in fact, they were

Received: June 11, 2019
Accepted: July 8, 2019
Published: July 8, 2019

Downloaded via MIAMI UNIV on October 22, 2019 at 02:39:15 (UTC).
See https://pubs.acs.org/sharingguidelines for options on how to legitimately share published articles.

© 2019 American Chemical Society

DOI: 10.1021/acsami.9b10176
ACS Appl. Mater. Interfaces 2019, 11, 27259−27268

very difficult to be used for multicolor biomedical imaging in vivo and in vitro. How to achieve ultrabright full color CDs by a simple and controllable method is still a bottleneck in this research field. Therefore, it is highly desirable to develop a suitable approach to improve the application value of CDs in various fields.

In this study, using an innovative hydrothermal method, two new CNCs with different crystal morphologies (branch-chain young sprout form (CM1) and conifer-pine form (CM2)) were first synthesized by fine polar manipulation. The morphologies of the CNCs from a simple compound were controlled availably. The growth mechanism of branched chains with two morphologies was well explored by a series of characterization analysis. The CNCs possess many outstanding advantages, such as nonluminescence themselves (from visible to ultraviolet), long-term preservation, and nearly no oxidization or deterioration at room temperature. The UBFCCDs can be prepared successfully by dissolving the CNCs in the corresponding polar solvents. By that, the as-prepared CDs show properties of multiexcitation, multi-emission, and higher intensity of photoluminescence (PL), which can be used for live biomedical imaging in vivo and in vitro and metal ion sensing.

2. EXPERIMENTAL SECTION

2.1. Materials. 1,5-Diaminonaphthalene (1,5-NDA) were purchased from Sigma. Absolute ethanol (≥99.7%), methanol (≥99.5%), acetone (≥99.5%), tetrahydrofuran (THF, ≥95%), and dimethyl sulfoxide (DMSO, ≥99.5%, Sigma D-4879) as the solvents were from Biosharp. The metal chlorates used for testing were supplied by Aladdin Corporation. All chemicals were of analytical reagent grade and used as received without further purification. Ultrapure water was purified with a Millipore system. A light-emitting diode (LED) was ordered from Australia, and its parameters were a voltage of 3.7 V, current of 20 mA, ID of 5 mm, wavelength of ±2 nm, and divergence angle of ≤30°.

2.2. Fine-Controlling Synthesis of the Carbon Nanocrystal Morphology. A single compound 1,5-NDA (0.18 g) was dissolved in 40 mL of the solution containing ultrapure water and ethanol under vigorous mixing. Afterward, the reaction solution was infused into a poly(tetrafluoroethylene) Teflon-lined autoclave and heated to 190 °C in the oven (12 h). Subsequently, the product solution was removed, sealed in a beaker, and naturally cooled to room temperature. The crystal was obtained as the sedimentation precipitated out. When the crystal in the beaker no longer precipitated out with its length and number reaching a plateau, the aged crystal was collected by filtering, rinsed with ultrapure water three to five times, and dried in vacuum at 25 °C.

2.3. Preparation of the Ultrabright Full Color Carbon Dots. By fine-controlling the volume ratio of the reactive solvents, two crystals with different morphologies were obtained successfully: CM1 with branch-chain young sprout form (H_2O/EtOH (22/18, v/v)) and CM2 with conifer-like form (H_2O/EtOH (26/14, v/v)). The ultrabright full color CDs could be easily obtained by dissolving the above dry crystals in different solvents at room temperature.

2.4. Characterizations. A JEOL JEM-2100F high-resolution transmission electron microscope (HR-TEM) and FEI Tecnai F30 were utilized to investigate the morphologies of as-prepared CDs. Atomic force microscopy (AFM) was carried out by a Nanoscope V Multimode 8 scanning probe microscope from Bruker Corporation. UV−vis absorption spectra were recorded on a Hitachi 3010 UV−vis spectrometer. A Fluorolog-3 (HORIBA Jobin Yvon) spectrometer was employed to study the emission spectra, fluorescence lifetimes, and up-conversion fluorescence experiments of samples. Quantum yields (QYs) were measured by an Edinburgh FLS 920. X-ray photoelectron spectroscopy (XPS) was conducted with an Escalab 250 XI spectrometer equipped with Al Kα radiation (1486.6 eV). The FT-IR spectroscopy data were obtained with a WQF-510A FT-IR spectrometer. Raman spectra were determined on a Raman spectrometer (Renishaw InVia) with 532 nm laser wavelength. The cell imaging was performed with a confocal laser fluorescence microscope (LSCM, Olympus, 405 nm, 454 nm, and 546 nm). Larvae were microinjected by an Eppendorf electric microinjector (FemtoJet 4i) and SZ760 series stereo microscope (Chongqing Optec Instrument Co., Ltd., China).

2.5. Video of Crystallization Process. Two drops of both CD solutions are taken on glass slides, and then the crystallization processes of both crystals were naturally recorded by CCD on a microscope along with solvent evaporation. When both kinds of crystals were dissolved in solvents, they turned into their respective CD solutions. In reverse, after solvent evaporation, both crystal forms emerged again. This process can be easily reproduced and recycled many times.

2.6. Cytotoxicity Assay. The cytotoxicity of as-prepared CDs against human cervical carcinoma (HeLa) cells was evaluated by the MTT assay. The HeLa cells were seeded in duplicate and incubated (5% CO_2, at 37 °C) for 24 h. Subsequently, the cells ingested 100 mL of Dulbecco's modified Eagle's medium (DMEM) containing CDs with gradient concentrations (25, 50, 75, 100, 125, 150, 175, and 200 μg/mL) and was allowed to adhere for 24 h. After incubating the cells for an additional 4 h and addition of 10 μL of MTT solution (5 mg/mL in PBS), the culture medium from each well was carefully withdrawn and formazan was solubilized by DMSO (10 μL). Finally, the optical density was measured at 550 nm using a microplate reader (Infinite M200 PRO Tecan). Triplicate measurements were performed to obtain a precise result. The percentage viability was calculated by the following equation

$$\text{cell viability}(\%) = (OD_{\text{sample}}/OD_{\text{control}}) \times 100 \quad (1)$$

where OD_{sample} and OD_{control} are optical densities of cells in the presence and absence of as-prepared CDs at 546 nm, respectively.

2.7. Cellular Imaging. DMEM containing 10% fetal bovine serum (FBS) and 1% penicillin−streptomycin solution was utilized as the medium. The HeLa cells (4×10^4 cells/mL) were seeded in duplicate and incubated in the medium (5% CO_2, at 37 °C) for 24 h. The cells was cultured with the CDs dispersed in DMEM (50 μg/mL) for 6 h and then washed three times with PBS to remove the free CDs. The cell images were observed by CLSM.

2.8. Ethics Statement. All animal experiments were performed in accordance with the guiding principles for the care and use of laboratory animals and were approved by the Animal Care Committee of Chongqing Institute of Green and Intelligent Technology, Chinese Academy of Sciences (Approval ID: ZKCQY0112).

2.9. Zebrafish Maintenance and Embryo Collection. Zebrafish maintenance and embryo collection were performed according to the standard maintenance and husbandry protocols. Briefly, the wild-type adult zebrafish were cultured with the 14:10 light/dark cycle at 28.5 °C. The fish were fed twice daily with freshly hatched brine shrimps (Brine Shrimp Direct, USA). One male and two female zebrafish were transferred to a breeding tank at night before the start of breeding. The next morning, sufficient embryos were collected within 30 min from the breeding tanks after the light was switched on, and then the embryos were washed using deionized water. After 4 h of post-fertilization (hpf), the embryos were examined under a dissecting light microscope (SZ760), and then normally developed embryos were selected for further experiments.

2.10. Larvae Microinjection and in Vivo Imaging. The typically developing zebrafish larvae were picked out and cultured in 5 mL of embryo medium supplemented with 1-phenyl-2-thiourea (PTU) in 6 well plates for 24 h at 28.5 °C. By means of the electric microinjector and stereo microscope, the larvae were microinjected with the CDs dispersed in sterile deionized water (50 μg/mL), cultured for 3 h, and then imaged by CLSM.

2.11. Multidimensional Sensing and Selectivity Detection on Metal Ions. In the experiment, the CM1 was dissolved in alcohol (50%) to test the FL quenching or enhancing effect caused by some metal ions. The fluorescence intensities of CDs (0.1 mg/mL, in 400

DOI: 10.1021/acsami.9b10176
ACS Appl. Mater. Interfaces 2019, 11, 27259−27268

μL PBS, 0.01 M, pH 7.4) under excitation at 375 nm were measured and recorded in the absence and presence of various metal ions (10^{-2} mol/L, Na^+, K^+, Mn^{2+}, Ag^+, Cd^{2+}, Pb^{2+}, Zn^{2+}, Co^{2+}, Ni^+, Fe^{2+}, and Mg^{2+}). Among these metal ions, Ag^+ only showed an obvious quenching effect. All experiments above were carried out at room temperature.

3. RESULTS AND DISCUSSION

As is shown in Scheme 1a–h, the carbon nanocrystals with two different morphologies (branch-chain young sprout form (Scheme 1b, CM1) and conifer-pine form (Scheme 1c, CM2)) were synthesized by a novel hydrothermal reaction using a single compound 1,5-diaminonaphthalene (1,5-NDA) as the carbon precursor (Scheme 1a). The growth process of the branched chain by fine-controlling two CNCs was recorded in real time, as is shown in Movies S1 and S2. Lattice structures of both crystal shapes belong to body-centered orthorhombic (Scheme 1d,e) from data of XRD and Jade 6.5 software. The obtained CNCs themselves show no fluorescence, but they can become ultrabright full color fluorescence CDs in corresponding polar solvents (Scheme 1f). One of them can show unique up-conversion luminescence characteristics under a lower excitation wavelength of 660 nm. The as-prepared CDs present promising implications for multicolor bioimaging in vivo and in vitro on the strength of their good PL characteristics (Scheme 1g,h) and as a good sensor to detect Ag^+ (Figure S10).

Scheme 1. Schematic Illustration of Property Characterizations for As-Prepared UBFCCDs[a]

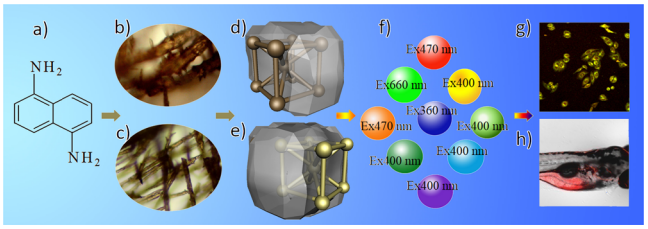

[a](a) Precursor of UBFCCDs. (b) Crystal morphology (young sprout form) of CM1. (c) Crystal morphology (conifer-pine form) of CM2. (d,e) Lattice structures of both crystal shapes. (f) Illustration of UBFCCDs under corresponding excitation wavelength. (g,h) Schematic illustrating the application of UBFCCDs in live bioimaging.

3.1. Shape and Morphology of the As-Prepared CNCs. The shape and morphology of the as-prepared CNCs were characterized by optical microscopy (Figure 1a,b) and scanning electron microscopy (SEM) (Figure 1c,d). It was obviously seen that CM1 was of branch-chain young sprout form and CM2 looked like conifer-pine form, which were also videotaped in Movies S1 and S2, respectively, during the process of crystal growth. Meanwhile, the two CNCs exhibiting nonluminance in the entire UV–visible region (Figure S1a–f) could form excitation-dependent multicolor CDs when they were dispersed in the solvent. On the contrary, the CDs restored to form crystals after the solvent evaporated. The cycle could repeat many times, but the FL intensity of the CD solution still did not show obvious weakening (Figure S2), which implied that the obtained CNCs might be well used for the development of intelligent light-controlled materials, smart probe, and sensing. In addition, from Figure S3, the CNCs were stored in the refrigerator (4 °C) for nearly 20 months, but the as-prepared CDs from the CNCs did not show much the fluorescence decay (CM1: 15.7% and CM2: 23.6%). There were even no oxidation metamorphism and bleaching for CNCs without special care (Figure S3). The aging test also indicated that the obtained CNCs possessed remarkable advantages of stable chemical properties and potential value for industrial application.

3.2. PL Emission, UV, and UCPL of As-Prepared Ultrabright Full Color Carbon Dots (UBFCCDs). From Figure 2a, we can clearly see multiwavelength emission, including red (Ex: 470 nm), orange (Ex: 470 nm), yellow (Ex: 400 nm), green (Ex: 400 nm), blue (Ex: 360 nm), violet (Ex: 380 nm), up-conversion green (Ex: 660 nm), and yellow-green (Ex: 660 nm). All the CDs can be adequately excited by

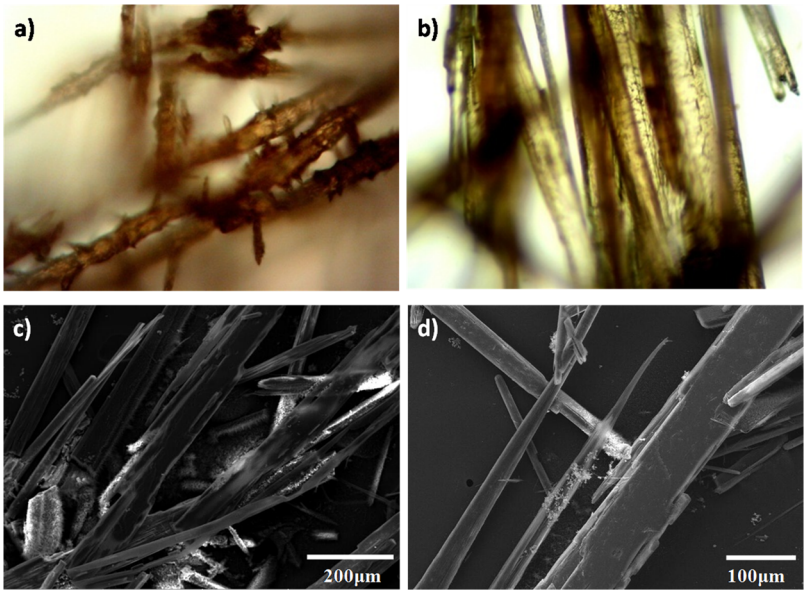

Figure 1. (a,b) Drop microscope photos of two kinds of as-prepared CNCs with different morphologies (CM1 and CM2); (c,d) SEM images of both kinds of as-prepared CNCs with different morphologies (CM1 and CM2).

DOI: 10.1021/acsami.9b10176
ACS Appl. Mater. Interfaces 2019, 11, 27259–27268

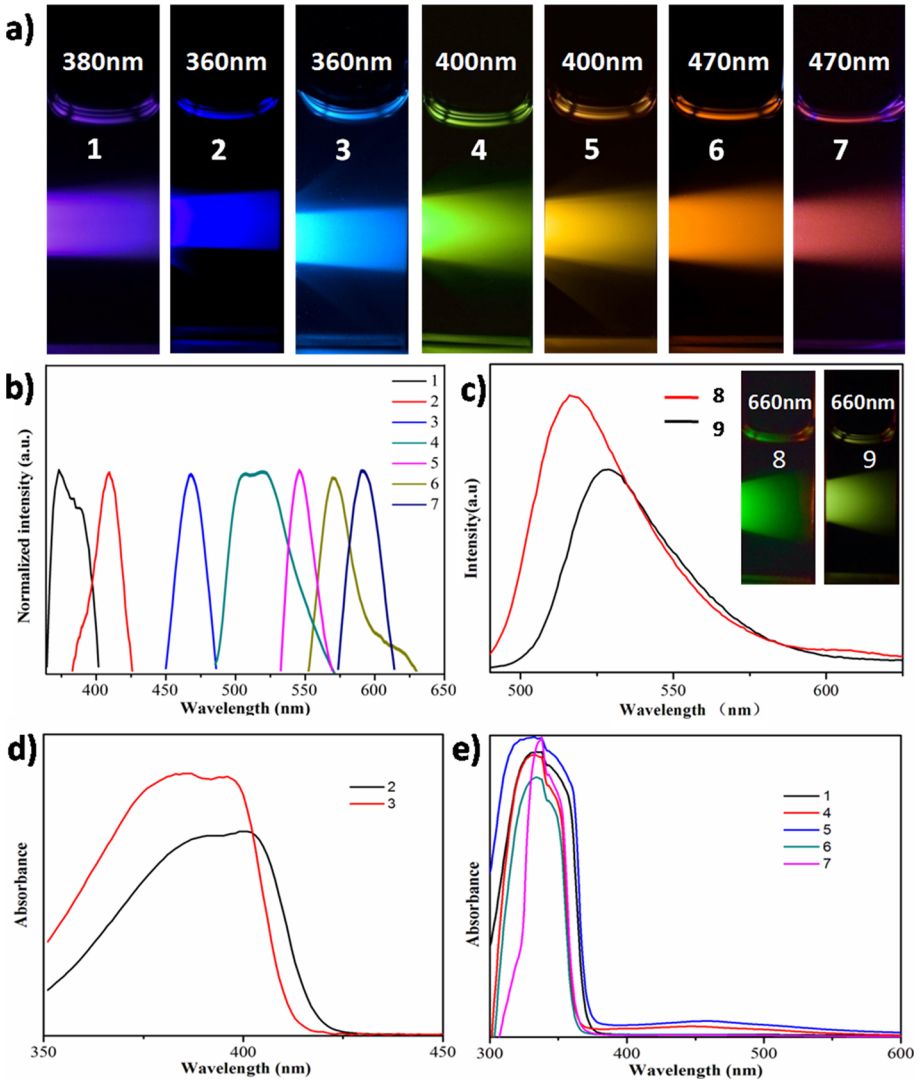

Figure 2. (a) PL emission photographs of as-prepared UBFCCDs (1−7). Under corresponding excitation wavelengths of LED, these UBCDs were obtained by adjusting the two kinds of crystal morphologies; CM1 was dissolved in DMSO (Nos. 1 and 5) and THF (Nos. 4 and 6); CM2 was dissolved in alcohol (Nos. 2 and 3) and acetone (No. 7); (b−e) PL and UV absorption spectra of CDs (1−7) under different excitation wavelengths; (8−9) UCPL spectra and photographs (insets) of CD1 under LED (Ex: 660 nm), which was prepared by dissolving CM1 in THF and DMSO, respectively.

some feeble LEDs instead of a fierce laser (Figure 2a). The optical properties of as-prepared CDs were characterized by UV−vis absorption and fluorescence spectra. The fluorescence spectra (Figure 2b,c) shows multiemission wavelengths at 597 (red), 592 (orange), 563 (yellow), 533 (green), 385 (blue), and 378 nm (purple) under corresponding ultraviolet spectra (Figure 2d,e). The inset in Figure 2c shows that the strongest peak of up-conversion luminescence (UCPL) is near 530 nm, emitting distinct green fluorescence in tetrahydrofuran and dimethyl sulfoxide solvents under an excitation wavelength of 660 nm. The as-prepared CDs show great advantages of optical properties of multiexcitation/emission and UCPL. The above feature indicates that the CDs can be used not only for noninvasive deep-tissue fluorescence imaging (including dual-photon deep-tissue imaging) but also for surface bioimaging.

In order to acquire the optimal PL intensity of the CDs, the factors influencing the PL intensity that involved the volume ratio of the reactive solvents and the reaction temperature were explored by fluorescence spectra of prepared CDs in aqueous solution. The corresponding results are shown in Figure S4. The optimized CD1 was obtained with a volume ratio of 22/18 of H_2O/EtOH at 180 °C for 12 h (Figure S4a,c). The optimized CD2 was obtained with a volume ratio of 26/14 of H_2O/EtOH at 200 °C for 12 h (Figure S4b,d). Both CD1 and CD2 exhibited multiemission and ultrabright full color fluorescence characteristics in different solvents at different excitation wavelengths (Figure S5). Besides, the two CDs showed different color fluorescence in the same solvent under the same excitation wavelength (Figure S6). The fluorescence intensities of the CD1/CD2 from the CNCs (CM1 and CM2) in aqueous solution reached the maximum at excitation wavelengths of 360 and 400 nm, respectively. At the same time, the corresponding fluorescence emissions of them were at 430 and 570 nm, respectively. The relevant fluorescence lifetime (τ) values were 5.35 and 8.49 ns, respectively (Figure S7, Table S1). The maximum fluorescence quantum yields (ΦF) of CD1 and CD2 were 48.8 and 78.0%, respectively, which are higher than those of traditional hydrothermal ways (41.5 and 69.0%, Table S2). The experimental details of measurements of CD quantum yields (QY%) were reported in

DOI: 10.1021/acsami.9b10176
ACS Appl. Mater. Interfaces 2019, 11, 27259−27268

our study before.[54] Regretfully, since we have not found a similar report about preparing the fine-controlling morphology or phase of CNCs to obtain the ultrabright full color CDs, we cannot compare their QY%.

3.3. Mechanism Exploration by FT-IR Spectra, XRD Pattern, TEM, AFM, XPS, and Raman. The surface functional groups of the CNCs were analyzed by FT-IR measurements. As displayed in Figure 3a, the intense bands at

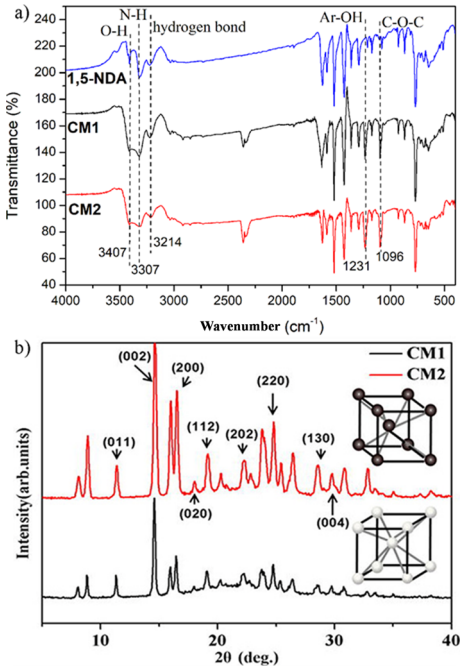

Figure 3. FT-IR spectra (a) and XRD pattern spectra (b) of as-prepared CDs and the precursor.

1450−1634 cm^{-1} were assigned to the stretching vibrations of the aromatic ring skeleton for the raw material (1,5-NDA) and the obtained CNCs (CM1 and CM2). Moreover, the bands of 3407, 3307, and 3214 cm^{-1} were attributed to the stretching vibrations of O−H, N−H, and hydrogen bonds, respectively, which were clearly seen in FT-IR spectra of all samples studied. However, compared to the FT-IR spectrum of 1,5-NDA, the absorption peaks at 1231 and 1096 cm^{-1} were attributed to the vibrations of Ar−OH and C−O−C of the CNCs, which revealed that 1,5-NDA was oxidized and underwent complex reactions during the hydrothermal carbonization. The N−H and O−H groups were conducive to the dispersity of the nanocrystals in the polar solvent.

On the other hand, why did two macroscopic shapes and morphologies of the CNCs obviously emerge by fine-controlling the solvent polarity? Following the query, the growth mechanisms of two kinds of CNCs were comprehensively studied with the help of FT-IR, XRD, XPS, Raman spectra, and so on. First, the crystalline structures of them were witnessed by XRD using Jade 6.5 software, as further illustrated by the index diagrams shown in Figure 3b. It was obviously seen that both crystalline phases belong to body-centered orthorhombic. The lattice parameters were a = 1.053 nm, b = 0.9739 nm, and c = 1.189 nm, including $\alpha = \beta = \gamma = 90°$. Generally speaking, for polar crystals, the polarity of the crystal interface is different. The interactions between the same or different solvents and the crystal interface are quite different. Even if the solvent is the same, the interactions between the solvent and the different crystal interfaces are still quite different, which changes the nature of the growth interface and influences the superimposed rate of growth units on the crystal interface, especially the positive and negative poles of crystals. Thus, the above results lead to different macroscopic morphologies of crystals. Because 1,5-NDA has different degrees of oxidation in EtOH/H_2O solvents with different volume ratios during the hydrothermal carbonization, the nanocrystals with different amounts of functional groups possess different polarities. The polarity of H_2O/EtOH (22/18, v/v) was less than the polarity of H_2O/EtOH (26/14, v/v), which caused that CM1 grew in both directions of axis c and exhibited the branch-chain young sprout form. As for CM2 with conifer-pine form, the increase of water content in solvents naturally restrained the growth of crystal planes (002) and (200) and improved the (011), (112), and (220) crystal plane growth. The (002) diffraction peak of CM1 was less than half as strong as that of CM2. The relative strengths of diffraction peaks of the (011), (112), and (220) crystal planes for CM2 increased from 19, 9.9, and 13.9% of CM1 to 22.5, 17.6, and 24.8%, respectively. In addition, the above results also exactly implied that the fluorescence intensity of CDs was changed by adjusting the volume ratio of water to ethanol in the synthetic process of CNCs.

Next, to reveal the morphologies of the UBFCCDs from CM1 and CM2, transmission electron microscopy (TEM) and atomic force microscopy (AFM) characterizations were carried out, as shown in Figure 4a−d. From the TEM images of the

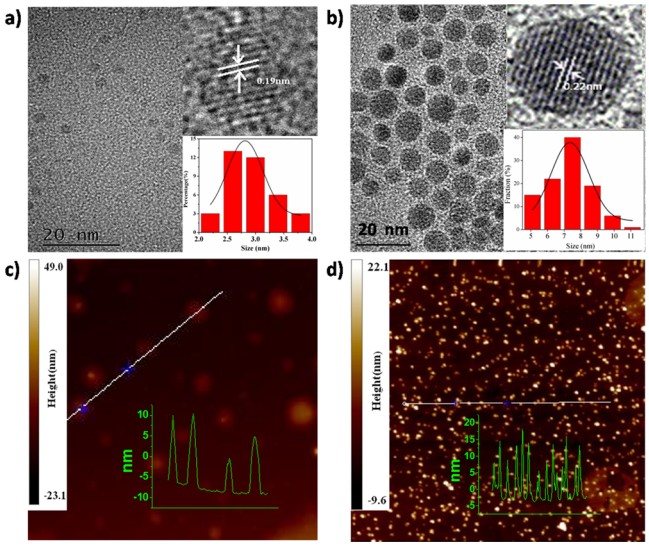

Figure 4. (a,b) TEM images of the UBFCCDs from two kinds of crystal morphologies (CM1 and CM2); red data: histograms and Gauss fittings of particle size distribution of the CDs; corresponding magnifications: HRTEM; (c,d) AFM images and height profile analysis of the UBFCCDs from two kinds of crystal morphologies (CM1 and CM2).

CDs from CM1 and CM2, it can be seen that the composition of nanoparticles is dispersed well and distributed uniformly (Figure 4a,b). Moreover, the shape is regular, showing a spherical shape. According to statistics, the average size distribution of the particle is near 9 nm. Furthermore, the high-resolution TEM examinations show that lattice fringes of the CDs from CM1 and CM2 can be clearly seen, and the

DOI: 10.1021/acsami.9b10176
ACS Appl. Mater. Interfaces 2019, 11, 27259−27268

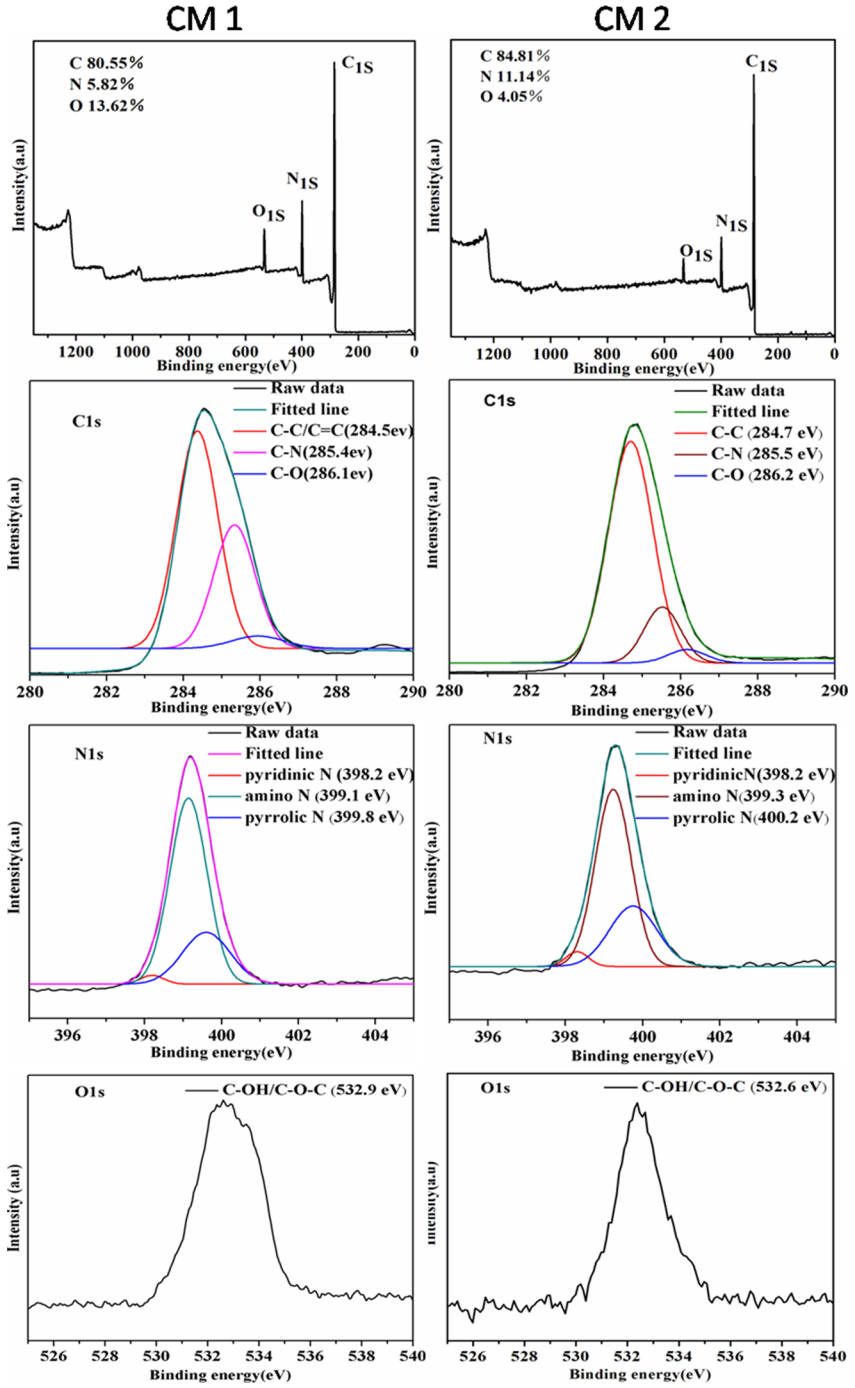

Figure 5. XPS survey, deconvoluted high-resolution XPS spectra, and the relative contents of C, N, and O atoms of the CM1 and CM2.

spacings of lattice bonds are 0.19 and 0.22 nm, respectively, which is consistent with the analytical results of the crystal plane from XRD. AFM images (Figure 4c,d) show that the CNCs become "ultrafine" nanoparticles (CDs) with diameters of 5−15 nm when they were dissolved in DMSO. The average diameter of particles is larger than that of our group's previously reported multicolor CDs.[55] Especially, the CD2 from CM2 shows different particle sizes with larger ratios (7.5 nm, 40%; 6.0 nm, 23%). Since the size of the luminescence particle can greatly affect the change of wavelength, exactly, the two scale distributions of CD2 caused the obvious doublet peaks.

Furthermore, X-ray photoelectron spectroscopy (XPS) was performed to characterize the CDs. As shown in Figure 5 (CM1 and CM2), the data of XPS confirm that the CDs from the two CM1 and CM2 exhibit the same element composition (i.e., C, O, and N), which contain C_{1S} (284.8 eV), N_{1S} (399.3 eV), and O_{1S} (532.41 eV). However, the two CNCs show different percentages of the atom content: C_{1S} (80.55%), N_{1S} (5.82%), and O_{1S} (13.62%) for CM1 and C_{1S} (84.81%), N_{1S} (11.14%), and O_{1S} (4.05%) for CM2. Their XPS spectra demonstrate that they exhibit the same chemical bonds (C−C/C=C, C−N, and C−O), as shown in Figure 5 (CM1 and CM2). However, the C_{1S} can further be divided into three C−C, C−N, and C−O bonds at bond energies of 284.7, 285.5,

DOI: 10.1021/acsami.9b10176
ACS Appl. Mater. Interfaces 2019, 11, 27259−27268

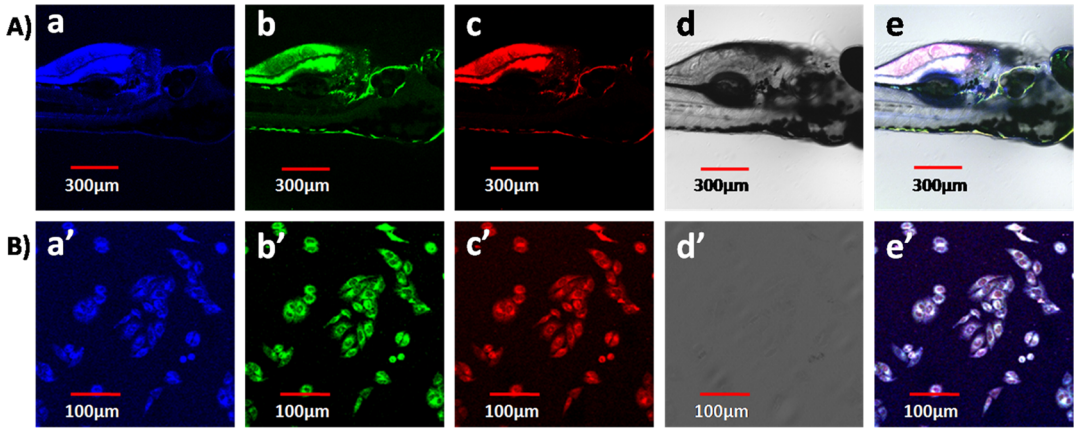

Figure 6. Confocal fluorescence images of the ultrabright full color CDs in living zebrafish larvae microinjection (A) and HeLa cells (B).

and 286.2 eV. Similarly, N_{1S} can also be divided into 398.2, 399.3, and 400.2 eV, corresponding to pyridine nitrogen, amino nitrogen, and pyrrolidine nitrogen, respectively. O_{1S} can also be divided into 531.0 and 532.6 eV, corresponding to C=O and Ar−OH/C−O−C bonds, respectively (C_{1S}, N_{1S}, and O_{1S} for CM2 are shown in Figure 5). There are only slight differences between the two CNCs. The analysis above can benefit for understanding the different PL characteristics of the CDs partially; of course, it is necessary to further investigate the possible chemical mechanism. Therefore, we use Raman spectroscopy to analyze the CNCs in order to reveal the relevant mechanism, as shown in Figure S8. As we know, the relative strength of the D band is a reflection of the disorder degree of crystalline structure, representing the defects of the lattice. Nevertheless, the G band represents the first-order scattering E_{2g}, which is a vibration mode in which two adjacent carbon atoms move in the opposite direction in the surface of a single-crystal graphene. The G band is equivalent to the E_{2g} mode of graphite that is related to the vibration of sp^2 hybridized carbon atoms in a two-dimensional hexagonal lattice.[56] The D/G strength ratio is a measurement method of disordered graphite; the D band is about 1350 cm^{-1}, and the G band is about 1590 cm^{-1}. However, the Raman spectra (Figure S8) imply that there are no obvious G and D bands in the CNCs, which implies that it cannot be the mode of graphite, but amorphous carbon. Furthermore, there are fewer defects and less disorder in the atomic crystals. The above results indicate that there are few carbon−carbon double bonds or carbon−carbon triple bonds in the crystals, which validated the above data of FT-IR.

3.4. Multicolor Live Biomedical Imaging in Vivo and in Vitro and Multidimensional Sensing for Metal Ions. To demonstrate the good biocompatibility of the as-prepared UBFCCDs, the cellular toxicity and imaging in vitro and in vivo were investigated preliminarily. The applications of the CDs can be expected to serve as potential multicolor biolabeling agents. The cytotoxicity of the CDs was evaluated by a standard MTT assay with HeLa cells. As shown in Figure S9, over 80% cell viabilities are observed after the incubation of HeLa cells with the CDs at concentrations ranging from 0 to 200 μg/mL for 24 h, confirming the low cytotoxicity of these PL materials. To reveal the potential applications of these CDs in multiplexed bioimaging, live cellular and zebrafish imaging in vitro and in vivo were preliminarily investigated (Figure 6A,B). After incubating the HeLa cells with each of the 50 μg/mL CDs for 6 h, the HeLa cells were imaged with a confocal microscope under excitation of 405, 454, and 546 nm lasers. The confocal micrographs exhibited different color emissions (Figure 6B), which suggested that the emissions of CDs mainly were located at the cytoplasmic regions and part regions of the nucleus. It is remarkable that CDs can not only pass through the cell membranes but also enter into the cell nucleus so that the entire cell regions show bright fluorescence (Figure 6Ba'−e'). The images demonstrate that the as-prepared CDs can be employed in multicolor biolabeling. More significantly, the CDs from CM2 are also found to exhibit the up-conversion emission property (Figure 2c, insets 8−9). This UCPL feature shows the further potential applications in surface layer bioimaging, besides deep-tissue PL imaging, including two-photon deep-tissue PL imaging.

Moreover, in order to study the biocompatibility of CDs and their interactions with zebrafish tissues, larvae microinjection and in vivo imaging were performed carefully. The embryos cultured for 5 days were changed to larvae and were microinjected with CD solution (50 μg/mL, 50 μL). The CDs were injected into the heart ventricles of larvae after fertilization (5 days). The zebrafish at this stage were selected because these fish were developing vertebrae and a benefit for experimental observations. Then the larvae were incubated at 28.5 °C for 24 h, and subsequently, their images were taken by the laser scanning confocal microscope under excitation of 405, 454, and 546 nm lasers, as shown in Figure 6A. These zebrafish images suggest strong fluorescence (red, green, and blue) in the entire zebrafish body, including skeletal structures such as vertebrae and cleithrum (Figure 6Aa−e). To the best of our knowledge, the practical tissue applications of full color CDs are reported for the first time.

Generally, the multidimensional methodology can show some advantages for the simultaneous detection and discrimination of multiple analytes. However, it is difficult to construct multidimensional sensing systems using traditional strategies due to their complex fabrication processes and many techniques to acquire satisfying PL signals, which may limit widespread applications of CDs. Thus, new design strategies based on multicolor CDs are still highly desirable for fabricating multidimensional sensing systems of metal ions. In the experiment, the CM1 was dissolved in alcohol (50%) to test the FL quenching or enhancing effect caused by these metal ions. As is shown in Figure S10, various metal ions (10^{-2} mol/L, Na^+, K^+, Mn^{2+}, Ag^+, Cd^{2+}, Pb^{2+}, Zn^{2+}, Co^{2+}, Ni^+, Fe^{2+}, and Mg^{2+}) were added into CD dispersion solution (0.1 mg/mL). Among these ions, most metal ions show quenching

DOI: 10.1021/acsami.9b10176
ACS Appl. Mater. Interfaces 2019, 11, 27259−27268

effects on CDs, but only Ag^+ can cause the great quenching effect on CDs. As for the PL quenching mechanism caused by Ag^+, it still needs to be studied further. These results clearly demonstrate that the as-prepared CDs could potentially be applied as a multimodal optical sensing platform for the detection and discrimination of multiple metal ions. Besides, the as-prepared CDs can be further explored as a probe to detect Ag^+.

4. CONCLUSIONS

In summary, using a single compound was reported to prepare the CNCs with two kinds of morphologies: branched chain sprouting and coniferous pine. The growth mechanism of the CNCs was explored deeply. Interestingly, the branched growth process of the label-free CNCs could be visualized in real time. Then, based on fine-controlling the CNCs, the UBFCCDs were easily obtained when the CNCs were dissolved in corresponding solvents. Nevertheless, after the solvents evaporated completely, the CNCs emerged again. The phenomenon can repeat many times, while the FL intensity of CDs from CNCs decreases hardly. The as-prepared CDs exhibit features of multiexcitation and multiemission (from blue to red) by fine polarity control and show unique up-conversion luminescence characteristics. Significantly, the QY (78%) of the as-prepared CDs is higher than that of the traditional hydrothermal method of dialysis and discarding precipitation (QY, 69.0%) at the same conditions. Moreover, the study fully utilized the atomic economy model. The full color CDs can be used for multicolor biomedical imaging in vivo and in vitro and sensing for metal ions. Particularly, the CNCs can be placed for a long time and shows better antioxidant without special care, which is of industrial significance.

■ ASSOCIATED CONTENT

Supporting Information

The Supporting Information is available free of charge on the ACS Publications website at DOI: 10.1021/acsami.9b10176.

Photos of the crystal morphologies; characterization data (PDF)

Growth process of CM1 (AVI)

Growth process of CM2 (AVI)

■ AUTHOR INFORMATION

Corresponding Authors

*E-mail: xiupeiyang@163.com (X.Y.).

*E-mail: zhaobin@nankai.edu.cn (B.Z.).

ORCID

Feng Huo: 0000-0002-3489-5055

Bin Zhao: 0000-0001-9003-9731

Xiupei Yang: 0000-0001-6799-5442

Notes

The authors declare no competing financial interest.

■ ACKNOWLEDGMENTS

This work was supported by the National Natural Science Foundation of China (Grant Nos. 21777130, 21277109, and 21625103), the Major Cultivation Project of Achievement Transformation (No. 16CZ02), the Talent Development Three Hundred Plan of Neijiang (RSC201701), and the Major Project of Science & Technology Department in Sichuan Province (No. 2016JY0168).

■ REFERENCES

(1) Li, J.; Wang, B.; Zhang, H.; Yu, J. Carbon Dots-in-Matrix Boosting Intriguing Luminescence Properties and Applications. *Small* **2019**, 1805504.

(2) Zhou, B.; Guo, Z.; Lin, Z.; Zhang, L.; Jiang, B. P.; Shen, X. C. Recent Insights into Near-Infrared Light-Responsive Carbon Dots for Bioimaging and Cancer Phototherapy. *Inorg. Chem. Front.* **2019**, *6*, 1116−1128.

(3) Tao, S.; Lu, S.; Geng, Y.; Zhu, S.; Redfern, S. A. T.; Song, Y.; Feng, T.; Xu, W.; Yang, B. Design of Metal-Free Polymer Carbon Dots: A New Class of Room-Temperature Phosphorescent Materials. *Angew. Chem., Int. Ed.* **2018**, *57*, 2393−2398.

(4) Ren, J.; Sun, J.; Sun, X.; Song, R.; Xie, Z.; Zhou, S. Precisely Controlled Up/Down-Conversion Liquid and Solid State Photoluminescence of Carbon Dots. *Adv. Opt. Mater.* **2018**, *6*, 1800115.

(5) Guo, Z.; Zhang, Z.; Zhang, W.; Zhou, L.; Li, H.; Wang, H.; Andreazza-Vignolle, C.; Andreazza, P.; Zhao, D.; Wu, Y.; Wang, Q.; Zhang, T.; Jiang, K. Color-Switchable, Emission-Enhanced Fluorescence Realized by Engineering C-dot@C-dot Nanoparticles. *ACS Appl. Mater. Interfaces* **2014**, *6*, 20700−20708.

(6) Li, D.; Jing, P.; Sun, L.; An, Y.; Shan, X.; Lu, X.; Zhou, D.; Han, D.; Shen, D.; Zhai, Y.; Qu, S.; Zbořil, R.; Rogach, A. L. Near-Infrared Excitation/Emission and Multiphoton-Induced Fluorescence of Carbon Dots. *Adv. Mater.* **2018**, *30*, 1705913.

(7) Li, S.; Guo, Z.; Zhang, Y.; Xue, W.; Liu, Z. Blood Compatibility Evaluations of Fluorescent Carbon Dots. *ACS Appl. Mater. Interfaces* **2015**, *7*, 19153−19162.

(8) Mintz, K. J.; Zhou, Y.; Leblanc, R. M. Recent Development of Carbon Quantum Dots Regarding their Optical Properties, Photoluminescence Mechanism, and Core Structure. *Nanoscale* **2019**, *11*, 4634−4652.

(9) Jing, S.; Zhao, Y.; Sun, R. C.; Zhong, L.; Peng, X. Facile and High-yield Synthesis of Carbon Quantum Dots from Biomass-derived Carbons at Mild Condition. *ACS Sustainable Chem. Eng.* **2019**, *7*, 7833−7843.

(10) Wei, X.; Li, L.; Liu, J.; Yu, L.; Li, H.; Cheng, F.; Yi, X.; He, J.; Li, B. Green Synthesis of Fluorescent Carbon Dots from Gynostemma for Bioimaging and Antioxidant in Zebrafish. *ACS Appl. Mater. Interfaces* **2019**, *11*, 9832−9840.

(11) Leturcq, R.; Stampfer, C.; Inderbitzin, K.; Durrer, L.; Hierold, C.; Mariani, E.; Schultz, M. G.; von Oppen, F.; Ensslin, K. Franck−Condon Blockade in Suspended Carbon Nanotube Quantum Dots. *Nat. Phys.* **2009**, *5*, 327−331.

(12) Hofmann, M. S.; Glückert, J. T.; Noé, J.; Bourjau, C.; Dehmel, R.; Högele, A. Bright, Long-Lived and Coherent Excitons in Carbon Nanotube Quantum Dots. *Nat. Nanotechnol.* **2013**, *8*, 502−505.

(13) Tsurugaya, T.; Yoshida, K.; Yajima, F.; Shimizu, M.; Homma, Y.; Hirakawa, K. Terahertz Spectroscopy of Individual Carbon Nanotube Quantum Dots. *Nano Lett.* **2019**, *19*, 242−246.

(14) Qing, Y.; Jiang, Y.; Lin, H.; Wang, L.; Liu, A.; Cao, Y.; Sheng, R.; Guo, Y.; Fan, C.; Zhang, S.; Jia, D.; Fan, Z. Boosting the Supercapacitor Performance of Activated Carbon by Constructing Overall Conductive Networks Using Graphene Quantum Dots. *J. Mater. Chem. A* **2019**, *7*, 6021−6027.

(15) Iannazzo, D.; Pistone, A.; Ferro, S.; de Luca, L.; Monforte, A. M.; Romeo, R.; Buemi, M. R.; Pannecouque, C. Graphene Quantum Dots Based Systems As HIV Inhibitors. *Bioconjugate Chem.* **2018**, *29*, 3084−3093.

(16) Ruan, J.; Wang, Y.; Li, F.; Jia, R.; Zhou, G.; Shao, C.; Zhu, L.; Cui, M.; Yang, D. P.; Ge, S. Graphene Quantum Dots for Radiotherapy. *ACS Appl. Mater. Interfaces* **2018**, *10*, 14342−14355.

(17) Dong, Y.; Wang, R.; Li, H.; Shao, J.; Chi, Y.; Lin, X.; Chen, G. Polyamine-Functionalized Carbon Quantum Dots for Chemical Sensing. *Carbon* **2012**, *50*, 2810−2815.

(18) Liu, H.; Li, R. S.; Zhou, J.; Huang, C. Z. Branched Polyethylenimine-Functionalized Carbon Dots as Sensitive and

Selective Fluorescent Probes for N-acetylcysteine via an OFF-ON Mechanism. *Analyst* **2017**, *142*, 4221−4227.
(19) Wang, F.; Liu, X. Multicolor Tuning of Lanthanide-Doped Nanoparticles by Single Wavelength Excitation. *Acc. Chem. Res.* **2014**, *47*, 1378−1385.
(20) Zheng, W.; Huang, P.; Tu, D.; Ma, E.; Zhu, H.; Chen, X. Lanthanide-Doped Upconversion Nano-Bioprobes: Electronic Structures, Optical Properties, and Biodetection. *Chem. Soc. Rev.* **2015**, *44*, 1379−1415.
(21) Schroeder, V.; Savagatrup, S.; He, M.; Lin, S.; Swager, T. M. Carbon Nanotube Chemical Sensors. *Chem. Rev.* **2019**, *119*, 599−663.
(22) Devi, P.; Thakur, A.; Chopra, S.; Kaur, N.; Kumar, P.; Singh, N.; Kumar, M.; Shivaprasad, S. M.; Nayak, M. K. Ultrasensitive and Selective Sensing of Selenium Using Nitrogen-Rich Ligand Interfaced Carbon Quantum Dots. *ACS Appl. Mater. Interfaces* **2017**, *9*, 13448−13456.
(23) Lu, W.; Jiao, Y.; Gao, Y.; Qiao, J.; Mozneb, M.; Shuang, S.; Dong, C.; Li, C. Z. Bright Yellow Fluorescent Carbon Dots as a Multifunctional Sensing Platform for the Label-Free Detection of Fluoroquinolones and Histidine. *ACS Appl. Mater. Interfaces* **2018**, *10*, 42915−42924.
(24) Sun, H.; Ren, J.; Qu, X. Carbon Nanomaterials and DNA: from Molecular Recognition to Applications. *Acc. Chem. Res.* **2016**, *49*, 461−470.
(25) Shangguan, J.; He, D.; He, X.; Wang, K.; Xu, F.; Liu, J.; Tang, J.; Yang, X.; Huang, J. Label-Free Carbon-Dots-Based Ratiometric Fluorescence PH Nanoprobes for Intracellular pH Sensing. *Anal. Chem.* **2016**, *88*, 7837−7843.
(26) Yang, W.; Ratinac, K. R.; Ringer, S. P.; Thordarson, P.; Justin Gooding, J.; Braet, F. Carbon Nanomaterials in Biosensors: Should You Use Nanotubes or Graphene? *Angew. Chem., Int. Ed.* **2010**, *49*, 2114−2138.
(27) Bartelmess, J.; Quinn, S. J.; Giordani, S. Carbon Nanomaterials: Multi-Functional Agents for Biomedical Fluorescence and Raman Imaging. *Chem. Soc. Rev.* **2015**, *44*, 4672−4698.
(28) Hong, G.; Diao, S.; Antaris, A. L.; Dai, H. Carbon Nanomaterials for Biological Imaging and Nanomedicinal Therapy. *Chem. Rev.* **2015**, *115*, 10816−10906.
(29) Anwar, S.; Ding, H.; Xu, M.; Hu, X.; Li, Z.; Wang, J.; Liu, L.; Jiang, L.; Wang, D.; Dong, C.; Yan, M.; Wang, Q.; Bi, H. Recent Advances in Synthesis, Optical Properties and Biomedical Applications of Carbon Dots. *ACS Appl. Bio Mater.* **2019**, 2317.
(30) Cha, C.; Shin, S. R.; Annabi, N.; Dokmeci, M. R.; Khademhosseini, A. Carbon-Based Nanomaterials: Multifunctional Materials for Biomedical Engineering. *ACS Nano* **2013**, *7*, 2891−2897.
(31) Zhang, S.; Kang, L.; Wang, X.; Tong, L.; Yang, L.; Wang, Z.; Qi, K.; Deng, S.; Li, Q.; Bai, X.; Ding, F.; Zhang, J. Arrays of Horizontal Carbon Nanotubes of Controlled Chirality Grown Using Designed Catalysts. *Nature* **2017**, *543*, 234−238.
(32) Qian, Z.; Shan, X.; Chai, L.; Ma, J.; Chen, J.; Feng, H. Si-Doped Carbon Quantum Dots: A Facile and General Preparation Strategy, Bioimaging Application, and Multifunctional Sensor. *ACS Appl. Mater. Interfaces* **2014**, *6*, 6797−6805.
(33) Zhu, S.; Meng, Q.; Wang, L.; Zhang, J.; Song, Y.; Jin, H.; Zhang, K.; Sun, H.; Wang, H.; Yang, B. Highly Photoluminescent Carbon Dots for Multicolor Patterning, Sensors, and Bioimaging. *Angew. Chem., Int. Ed.* **2013**, *52*, 3953−3957.
(34) Guo, J.; Liu, D.; Filpponen, I.; Johansson, L. S.; Malho, J. M.; Quraishi, S.; Liebner, F.; Santos, H. A.; Rojas, O. J. Photoluminescent Hybrids of Cellulose Nanocrystals and Carbon Quantum Dots as Cytocompatible Probes for in Vitro Bioimaging. *Biomacromolecules* **2017**, *18*, 2045−2055.
(35) Goh, E. J.; Kim, K. S.; Kim, Y. R.; Jung, H. S.; Beack, S.; Kong, W. H.; Scarcelli, G.; Yun, S. H.; Hahn, S. K. Bioimaging of Hyaluronic Acid Derivatives Using Nanosized Carbon Dots. *Biomacromolecules* **2012**, *13*, 2554−2561.
(36) Ding, H.; Wei, J. S.; Zhong, N.; Gao, Q. Y.; Xiong, H. M. Highly Efficient Red-Emitting Carbon Dots with Gram-Scale Yield for Bioimaging. *Langmuir* **2017**, *33*, 12635−12642.
(37) Lim, S. Y.; Shen, W.; Gao, Z. Carbon Quantum Dots and Their Applications. *Chem. Soc. Rev.* **2015**, *44*, 362−381.
(38) Zhang, X.; Zhang, Y.; Wang, Y.; Kalytchuk, S.; Kershaw, S. V.; Wang, Y.; Wang, P.; Zhang, T.; Zhao, Y.; Zhang, H.; Cui, T.; Wang, Y.; Zhao, J.; Yu, W. W.; Rogach, A. L. Color-Switchable Electroluminescence of Carbon Dot Light-Emitting Diodes. *ACS Nano* **2013**, *7*, 11234−11241.
(39) Wang, C. I.; Wu, W. C.; Periasamy, A. P.; Chang, H. T. Electrochemical Synthesis of Photoluminescent Carbon Nanodots From Glycine for Highly Sensitive Detection of Hemoglobin. *Green Chem.* **2014**, *16*, 2509−2514.
(40) Huang, H.; Cui, Y.; Liu, M.; Chen, J.; Wan, Q.; Wen, Y.; Deng, F.; Zhou, N.; Zhang, X.; Wei, Y. A One-Step Ultrasonic Irradiation Assisted Strategy for the Preparation of Polymer-Functionalized Carbon Quantum Dots and Their Biological Imaging. *J. Colloid Interface Sci.* **2018**, *532*, 767−773.
(41) Dang, H.; Huang, L. K.; Zhang, Y.; Wang, C. F.; Chen, S. Large-Scale Ultrasonic Fabrication of White Fluorescent Carbon Dots. *Ind. Eng. Chem. Res.* **2016**, *55*, 5335−5341.
(42) Costas-Mora, I.; Romero, V.; Lavilla, I.; Bendicho, C. In Situ Building of a Nanoprobe Based on Fluorescent Carbon Dots for Methylmercury Detection. *Anal. Chem.* **2014**, *86*, 4536−4543.
(43) Liu, H.; He, Z.; Jiang, L.-P.; Zhu, J.-J. Microwave-Assisted Synthesis of Wavelength-Tunable Photoluminescent Carbon Nanodots and Their Potential Applications. *ACS Appl. Mater. Interfaces* **2015**, *7*, 4913−4920.
(44) Rodríguez-Padrón, D.; Algarra, M.; Tarelho, L. A.C.; Frade, J.; Franco, A.; de Miguel, G.; Jiménez, J.; Rodríguez-Castellón, E.; Luque, R. Catalyzed Microwave-Assisted Preparation of Carbon Quantum Dots From Lignocellulosic Residues. *ACS Sustainable Chem. Eng.* **2018**, *6*, 7200−7205.
(45) Che, Y.; Pang, H.; Li, H.; Yang, L.; Fu, X.; Liu, S.; Ding, L.; Hou, J. Microwave-Assisted Fabrication of Copper-Functionalized Carbon Quantum Dots for Sensitive Detection of Histidine. *Talanta* **2019**, *196*, 442−448.
(46) Wang, T. Y.; Chen, C. Y.; Wang, C. M.; Tan, Y. Z.; Liao, W. S. Multicolor Functional Carbon Dots via One-Step Refluxing Synthesis. *ACS Sens.* **2017**, *2*, 354−363.
(47) Luo, B.; Hong, Y.; Li, D.; Fang, Z.; Jian, Y.; Shi, W. Fabrication of 0D/2D Carbon Nitride Quantum Dots/$SnNb_2O_6$ Ultrathin Nanosheets with Enhanced Photocatalytic Hydrogen Production. *ACS Sustainable Chem. Eng.* **2018**, *6*, 14332−14339.
(48) Xia, C.; Tao, S.; Zhu, S.; Song, Y.; Feng, T.; Zeng, Q.; Liu, J.; Yang, B. Hydrothermal Addition Polymerization for Ultrahigh-yield Carbonized Polymer Dots with Room Temperature Phosphorescence via Nanocomposite. *Chem. − Eur. J.* **2018**, *24*, 11303−11308.
(49) Liyanage, P. Y.; Graham, R. M.; Pandey, R. R.; Chusuei, C. C.; Mintz, K. J.; Zhou, Y.; Harper, J. K.; Wu, W.; Wikramanayake, A. H.; Vanni, S.; Leblanc, R. M. Carbon Nitride Dots: A Selective Bioimaging Nanomaterial. *Bioconjugate Chem.* **2019**, *30*, 111−123.
(50) Li, J. Y.; Liu, Y.; Shu, Q. W.; Liang, J. M.; Zhang, F.; Chen, X. P.; Deng, X. Y.; Swihart, M. T.; Tan, K. J. One-Pot Hydrothermal Synthesis of Carbon Dots with Efficient Up- and Down-Converted Photoluminescence for the Sensitive Detection of Morin in a Dual-Readout Assay. *Langmuir* **2017**, *33*, 1043−1050.
(51) Zhao, S.; Lan, M.; Zhu, X.; Xue, H.; Ng, T. W.; Meng, X.; Lee, C. S.; Wang, P.; Zhang, W. Green Synthesis of Bifunctional Fluorescent Carbon Dots from Garlic for Cellular Imaging and Free Radical Scavenging. *ACS Appl. Mater. Interfaces* **2015**, *7*, 17054−17060.
(52) Kameyama, T.; Ishigami, Y.; Yukawa, H.; Shimada, T.; Baba, Y.; Ishikawa, T.; Kuwabata, S.; Torimoto, T. Crystal Phase-Controlled Synthesis of Rod-Shaped $AgInTe_2$ nanocrystals for In Vivo Imaging in The Near-Infrared Wavelength Region. *Nanoscale* **2016**, *8*, 5435−5440.

DOI: 10.1021/acsami.9b10176
ACS Appl. Mater. Interfaces 2019, 11, 27259−27268

(53) Zhu, Y.; Bi, D.; Wang, H.; Wang, Y.; Xu, X.; Lu, Z.; Xu, W. Fine-Tuning of Multiple Upconversion Emissions by Controlling the Crystal Phase and Morphology between GdF_3: Yb^{3+}, Tm^{3+} and GdOF:Yb^{3+}, Tm^{3+} nanocrystals. *RSC Adv.* **2017**, *7*, 2426−2434.
(54) Huo, F.; Kang, Z.; Zhu, M.; Tan, C.; Tang, Y.; Liu, Y.; Zhang, W. Metal-triggered fluorescence enhancement of multicolor carbon dots in sensing and bioimaging. *Opt. Mater.* **2019**, *94*, 363−370.
(55) Huo, F.; Liang, W.; Tang, Y.; Zhang, W.; Liu, X.; Pei, D.; Wang, H.; Jia, W.; Jia, P.; Yang, F. Full-Color Carbon Dots with Multiple Red-Emission Tuning: ON/OFF Sensors, In Vitro and In Vivo multicolor Bioimaging. *J. Mater. Sci.* **2019**, *54*, 6815−6825.
(56) Li, H.; He, X.; Kang, Z.; Huang, H.; Liu, Y.; Liu, J.; Lian, S.; Tsang, C. H. A.; Yang, X.; Lee, S.-T. Water-Soluble Fluorescent Carbon Quantum Dots and Photocatalyst Design. *Angew. Chem., Int. Ed.* **2010**, *49*, 4430−4434.

DOI: 10.1021/acsami.9b10176
ACS Appl. Mater. Interfaces 2019, 11, 27259−27268